Supporting Information

Anti-bacterial, Anti-biofilm and Synergist Effects of Phenazinic-Based Ruthenium(II) Complexes

Patrícia H. R. Martins,[1] Adolfo I. B. Romo,[2] Florencio S. G. Júnior,[1] Iury A. Paz,[3] Nilberto R. F. Nascimento,[3] Alexandre L. Andrade,[4] Joaquín Rodríguez-López,[2] Mayron A. de Vasconcelos[5], Edson Holanda Teixeira[4], Carlos André Ferreira Moraes,[6] Luiz G. F. Lopes[1]*, Eduardo Henrique Silva Sousa[1]*

[1]Bioinorganic Group, Department of Organic and Inorganic Chemistry, Federal University of Ceará, Fortaleza, Ceará, Brazil, 60451-970.

[2]Department of Chemistry, University of Illinois at Urbana−Champaign, Urbana, Illinois, USA, 61801.

[3]Laboratory of Cardiovascular and Renal Physiology and Pharmacology (LAFCAR), State University of Ceará (UECE), Fortaleza, Ceará, Brazil, 60714-903.

[4]Biomolecule Integrated Laboratory (LIBS), Federal University of Ceará, Fortaleza, Ceará, Brazil, 60451-970.

[5]Faculty of Education of Itapipoca (FACEDI), State University of Ceará (UECE), Itapipoca, Ceará, Brazil, 62500-000.

6 Department of Chemistry, Federal University of São Carlos (UFSCar), São Carlos, São Paulo, Brazil, 13565-905

*Corresponding authors: eduardohss@dqoi.ufc.br and lopeslu@dqoi.ufc.br

Note 1: **PR** metal complex was characterized by FTIR spectrum that showed bands consistent with aromatic-based polypyridinic ligands with stretching of C-H and C=C bonds at 3064-2929 cm^{-1} and 1486 cm^{-1}, respectively (Figure S1). In addition, this compound exhibited a metal-to-ligand charge-transfer with maximum at 504 nm (MLCT band) noticed in similar systems containing a Ru(II) metal center (Figure S2). Cyclic voltammetry showed a reversible electrochemical process at $E_{1/2}$= 0.52V vs Ag|AgCl consistent to a $Ru^{III/II}$ process (Figure S3).

Note 2: **PR01** was also investigated by FTIR analysis that showed a nitrogen bound nitrite ligand with symmetric and asymmetric stretching $\nu(NO_2^-)$ at 1333-1353 cm^{-1} and also a typical sulfur bonded sulfite stretching mode $\nu(SO_3^-)$ at 1139 cm^{-1}. This profile is in agreement with theoretical measurements and analogous ruthenium complexes (e.g., *cis*-$[Ru(bpy)_2(SO_3)(NO)](PF_6)$.[1, 2] Electronic spectra in the UV-vis region for this metal complex showed a MLCT band with maximum at 405 nm in DMSO.

Note 3: For **PR02**, its stretching mode value for NO^+ was remarkably close to the ones (Figure S7) in *cis*-$[Ru(bpy)_2(SO_3)(NO)](PF_6)$ (at 1911 cm^{-1})[1] and *cis*-$[Ru(phen)_2(SO_3)(NO)](PF_6)$ (at 1913 cm^{-1})[3], even though a phenazinic ligand (dppz) was used instead. On the other hand, different monodentate ligands (L) bound to a *cis*-$[Ru(bpy)_2(L)(NO)]$ moiety can more expressively alter $\nu(NO^+)$. For example, $\nu(NO^+)$ for *cis*- $[Ru(bpy)_2(L)(NO)]$ was found at 1930, 1940, 1948 when using L = ethylenethiourea, 2-methylimidazole or isonicotinamide, respectively.[1, 4] These data would suggest that monodentated *cis*-ligand may cause a major disturbance on bound NO, but this is not completely true since other properties were expressively affected by using distinct bidentated polypiridinic ligands as further described for

PR02. These monodentate ligands could influence NO not only through an overall change in the electronic distribution but also through direct interactions due to proximity. Thus, a combination of effects may be responsible for the overall kinetic and thermodynamic properties of this type of ruthenium nitrosyl compound.

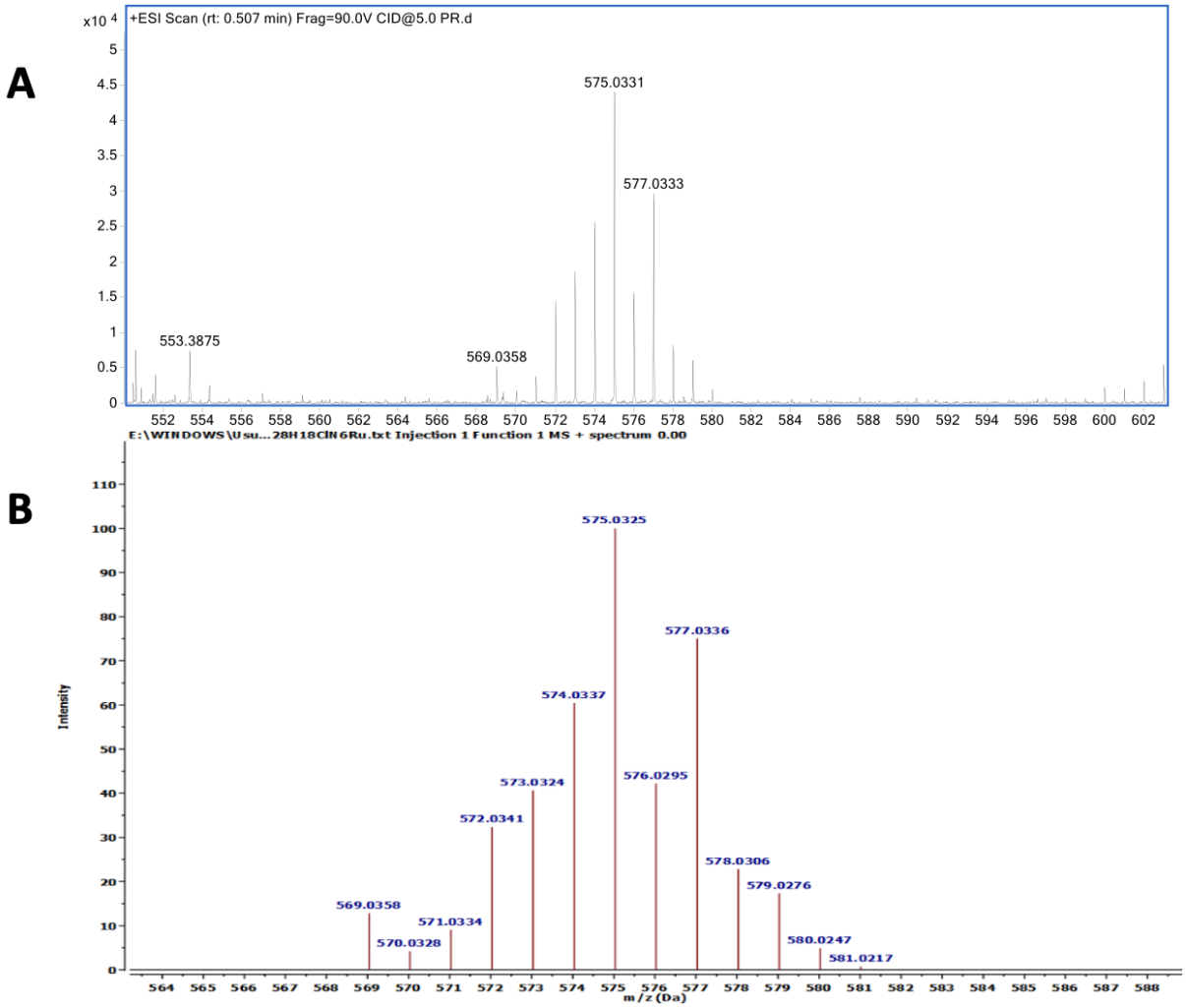

Figure S1. High-resolution mass spectrometry of **PR** in 1:1 methanol:acetonitrile, experimental (A) and calculated (B).

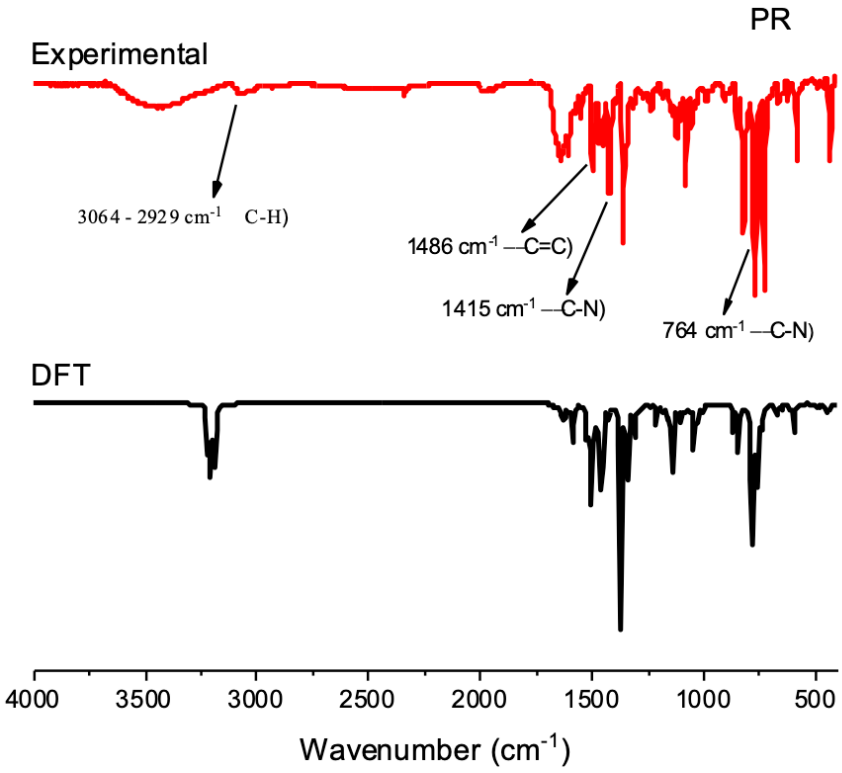

Figure S2. DFT-simulated (black) and experimental (red) FTIR spectra of **PR** complex in a KBr pellets.

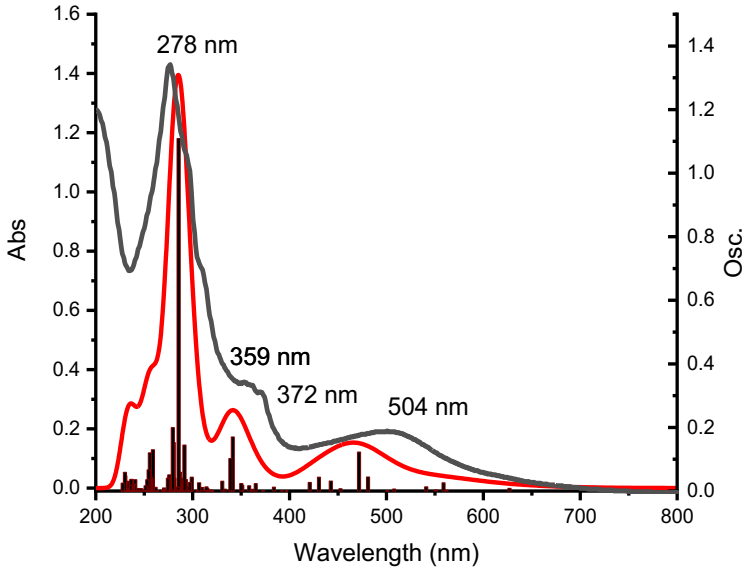

Figure S3. DFT-simulated (red) and experimental (gray) electronic spectra of of **PR** in DMSO.

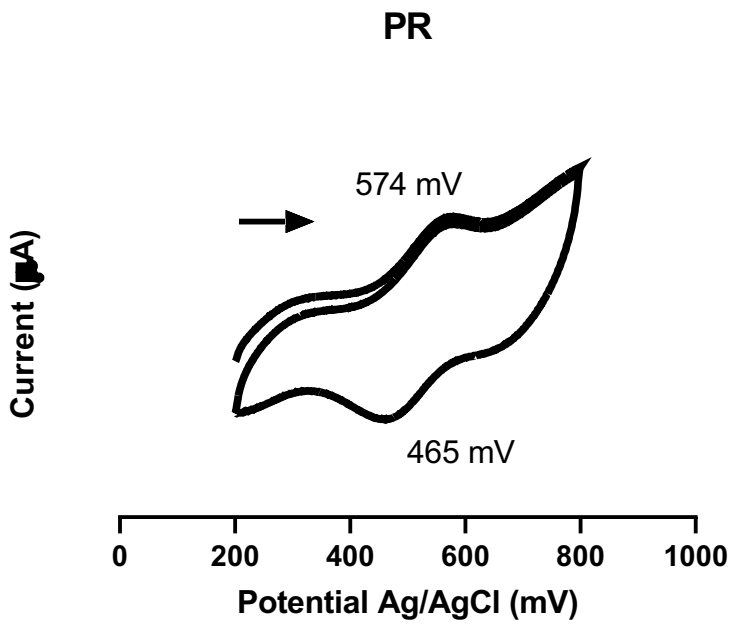

Figure S4 – Cyclic voltammogram of a DMF solution containing 2.0 x 10^{-6} mol L^{-1} of **PR** complex and 0.1 mol L^{-1} of PTBA. Measurement performed at 100 mVs^{-1}, and glassy carbon, platinum and Ag/AgCl electrode as working, counter and reference electrodes, respectively.

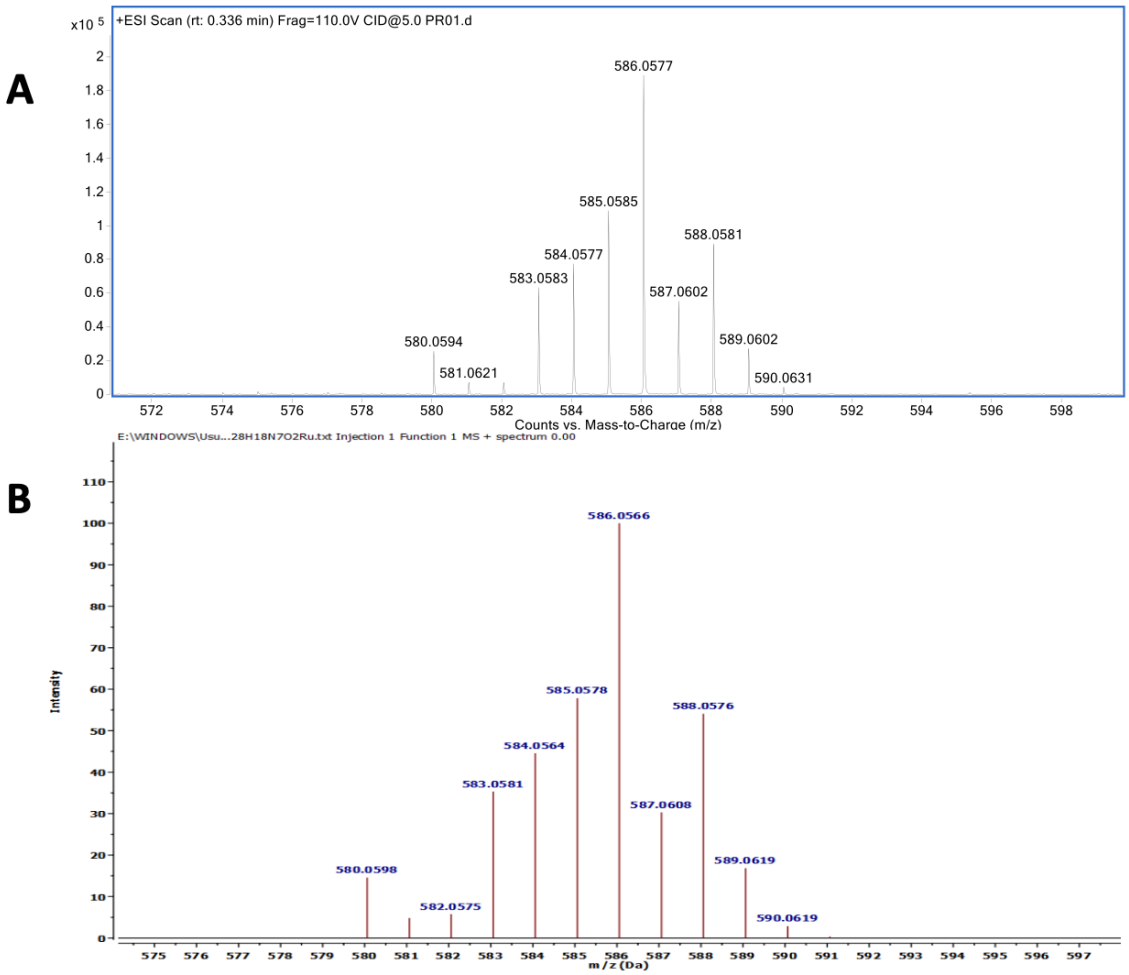

Figure S5. High-resolution mass spectrometry of **PR01** in 1:1 methanol:acetonitrile, experimental (A) and calculated (B).

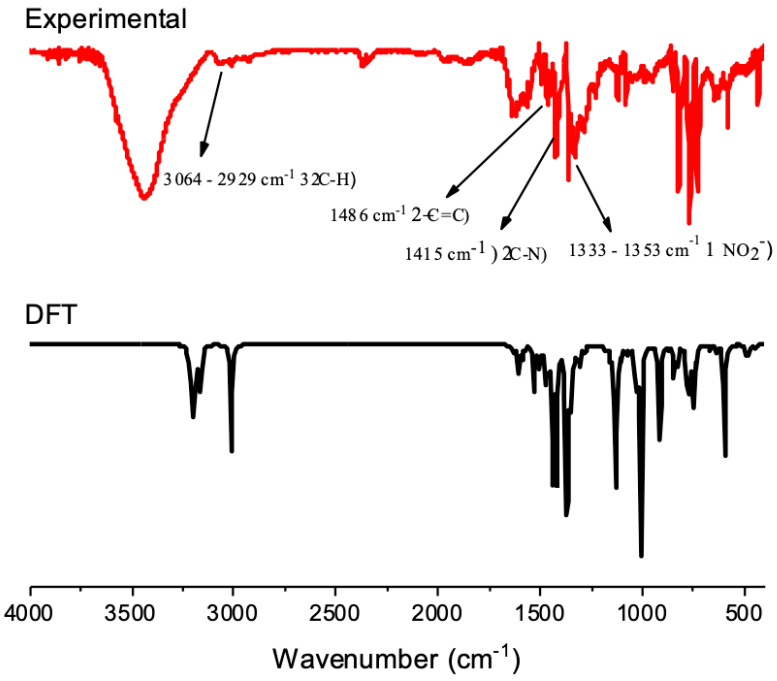

Figure S6. Infrared spectra simulated (black) and experimental (red) of a KBr pellets containing **PR01** complex.

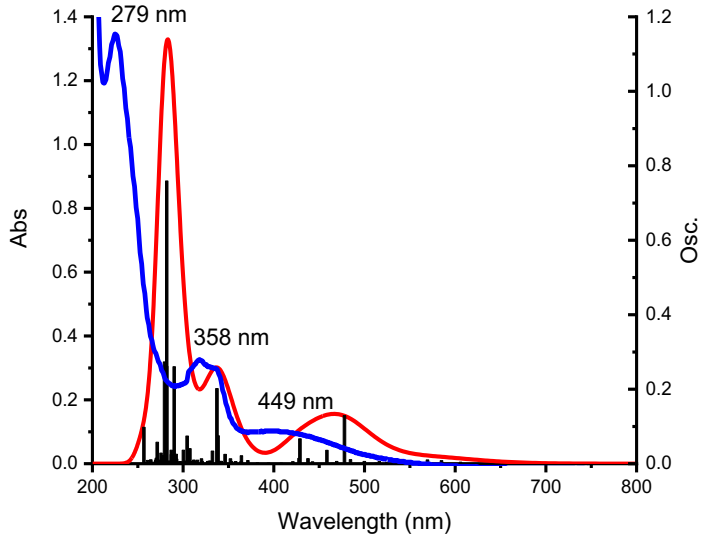

Figure S7. Simulated (red) and experimental (blue) electronic spectra of a DMSO solution containing 4.0 x 10^{-6} mol L^{-1} mol L^{-1} of **PR01** complex.

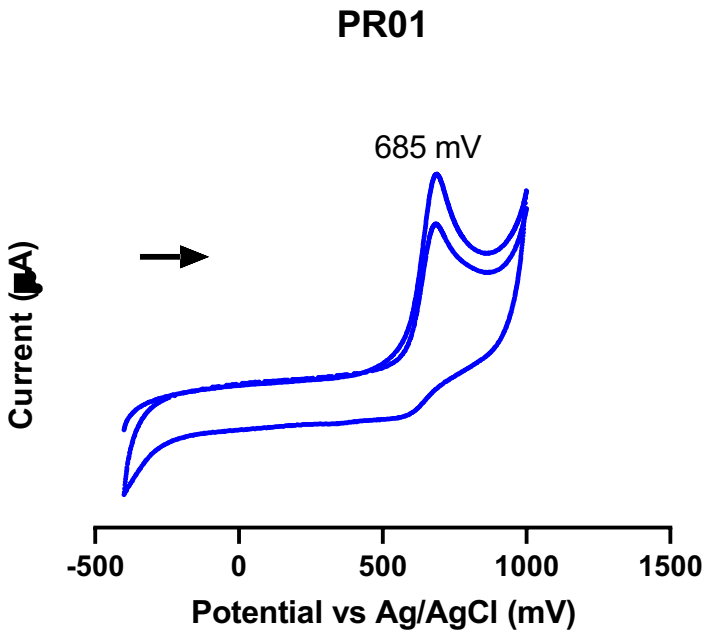

Figure S8. Cyclic voltammogram of a NaTFA 0.1 mol L^{-1} pH 4.0 aqueous solution containing 2.0 x 10^{-6} mol L^{-1} of **PR01** complex and 0.1 mol L^{-1} of PTBA. Measurement performed at 25 mV s^{-1}, used glassy carbon, platinum and Ag/AgCl electrodes as working, counter and reference electrodes, respectively.

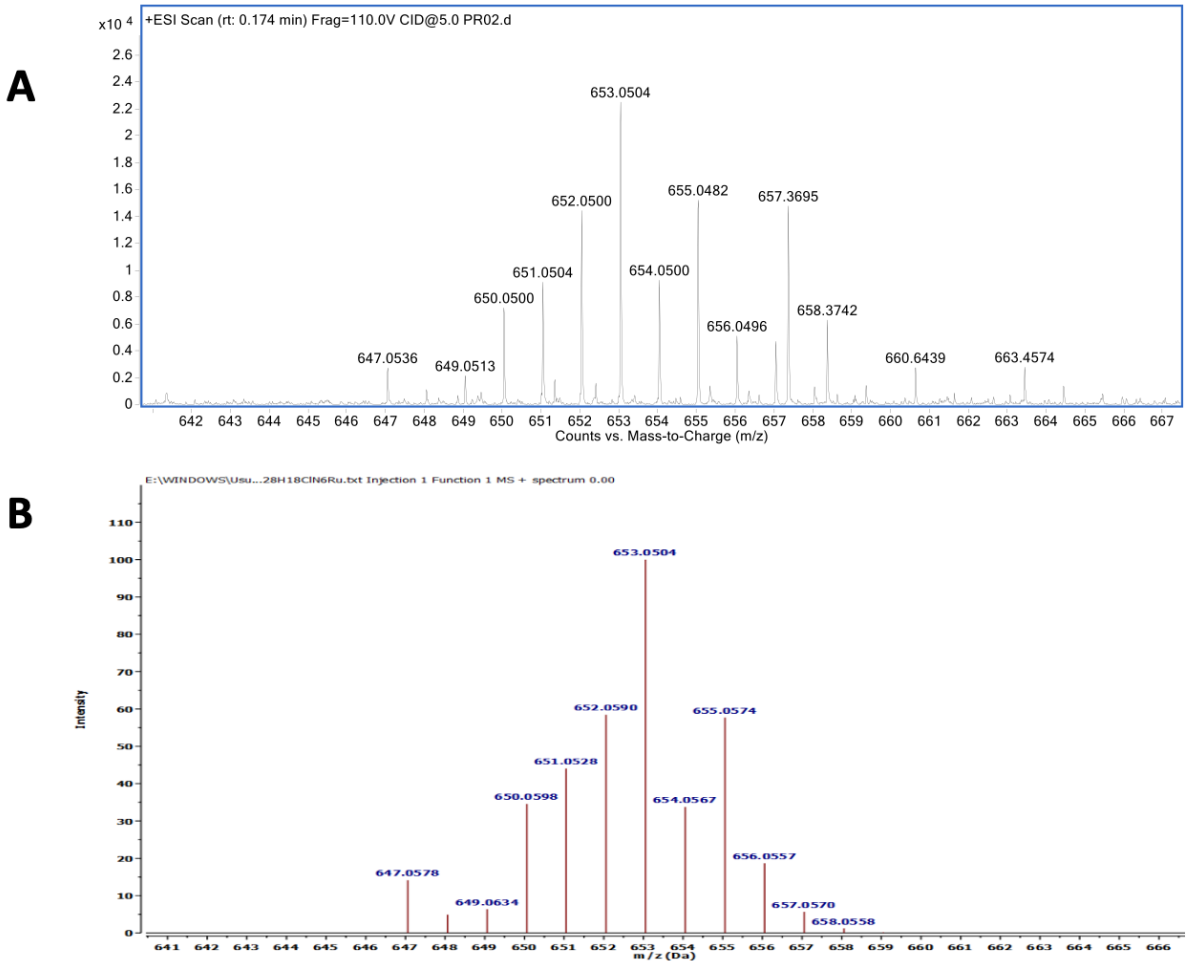

Figure S9. High-resolution mass spectrometry of **PR02** in 1:1 methanol:acetonitrile, experimental (A) and calculated (B).

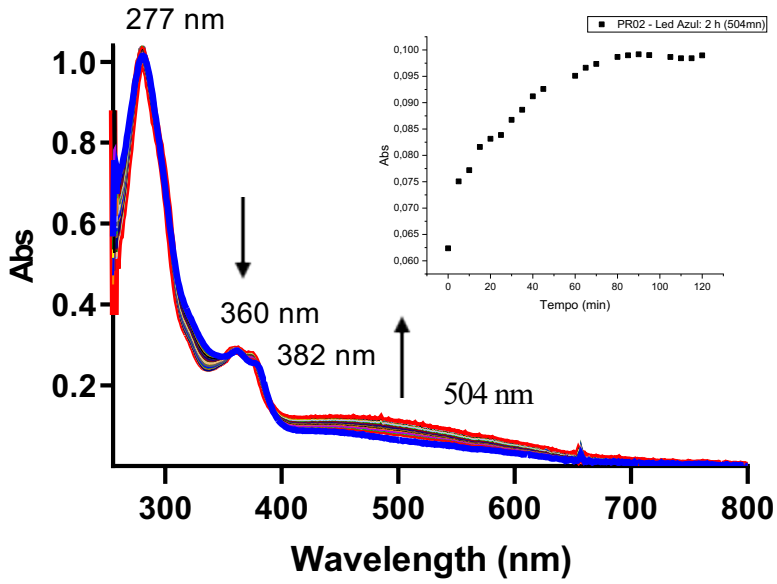

Figure S10. Kinetic study of the **PR02** at 17 µmol L^{-1} in 0.1 mol L^{-1} of phosphate buffer, pH 7.4, in the presence of 5 mmol L^{-1} of glutathione for 2 h at 37 °C.

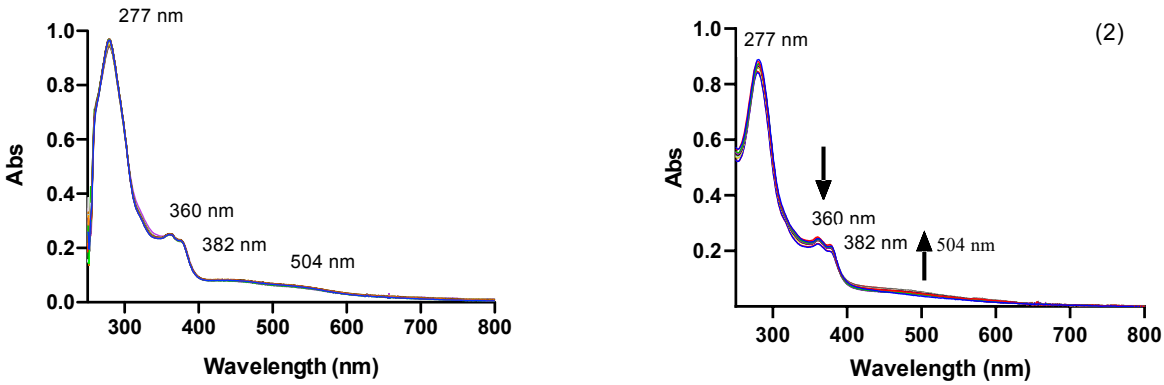

Figure S11. Kinetic study of the **PR02** complex at 20 µmol L^{-1} in phosphate buffer 0.1 mol L^{-1} pH 7.4 in 5% DMSO with (left image) and without light (right image), monitored for 2h.

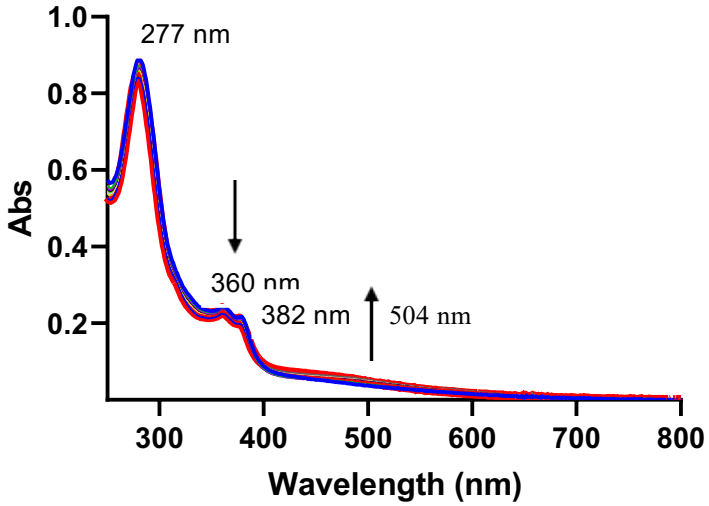

Figure S12. Kinetic study of the **PR02** complex at 20 µmol L^{-1} in NaTFA 0.1 mol L^{-1} at pH 1.6 irradiated for 2 h with blue LED.

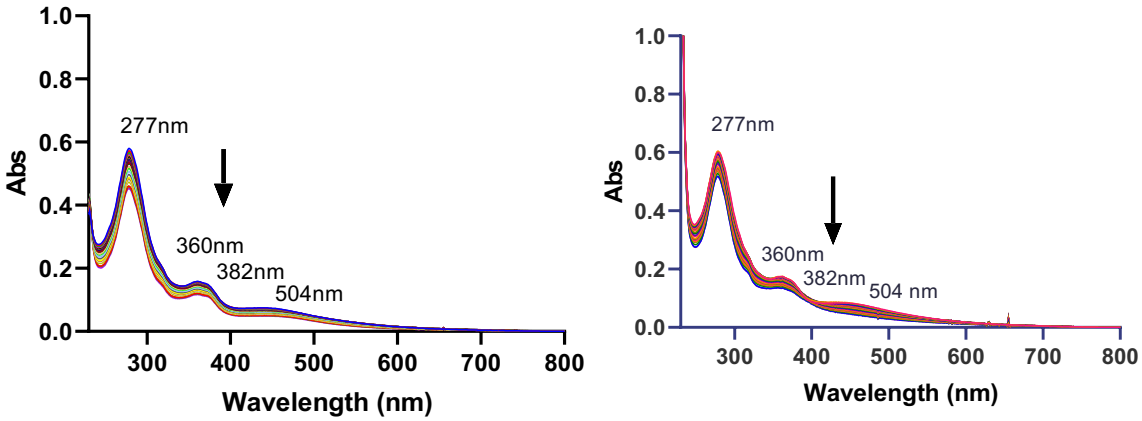

Figure S13. Thermal stability study of **PR02** at 8.5 µmol L^{-1} in 0.1 mol L^{-1} of phosphate buffer pH 7.4 and 5% DMSO without (left image) and with (right image) blue LED irradiation (λ_{max} = 463 nm) for 720 min (12h) at 37ºC (2).

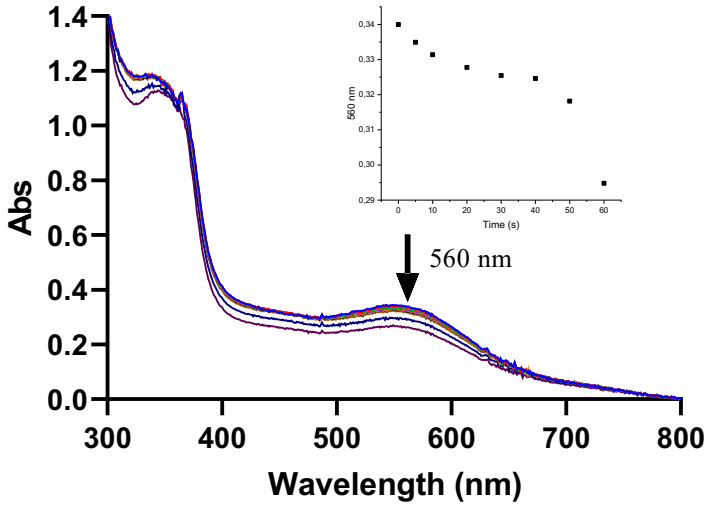

Figure S14. Study of NO/HNO release monitored by the reaction of **PR02** at 100 µmol L^{-1} with 190 µmol L^{-1} of cPTIO, in 0.1 mol L^{-1} of phosphate buffer pH 7.4. Inset: Monitoring absorbance changes over time up to 60 min, then added glutathione.

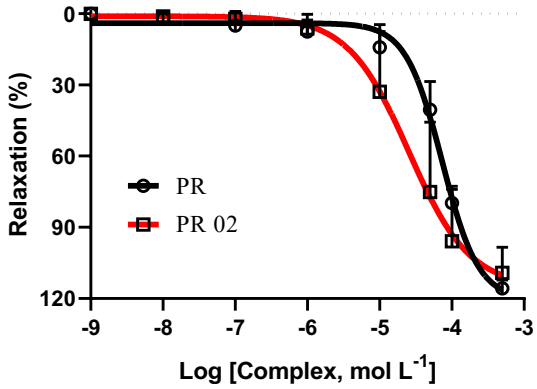

Ru complex	EC_{50} (µmol L^{-1})
cis-$[Ru(bpy)_2(SO_3)NO](PF_6)_3$	0.037
PR	73.0
PR02	25.0

Figure S15. Dose-response curves for vasodilation assay in rat aorta using **PR** and **PR02** complexes. Relaxation responses are expressed as percent relaxation versus complex concentration.

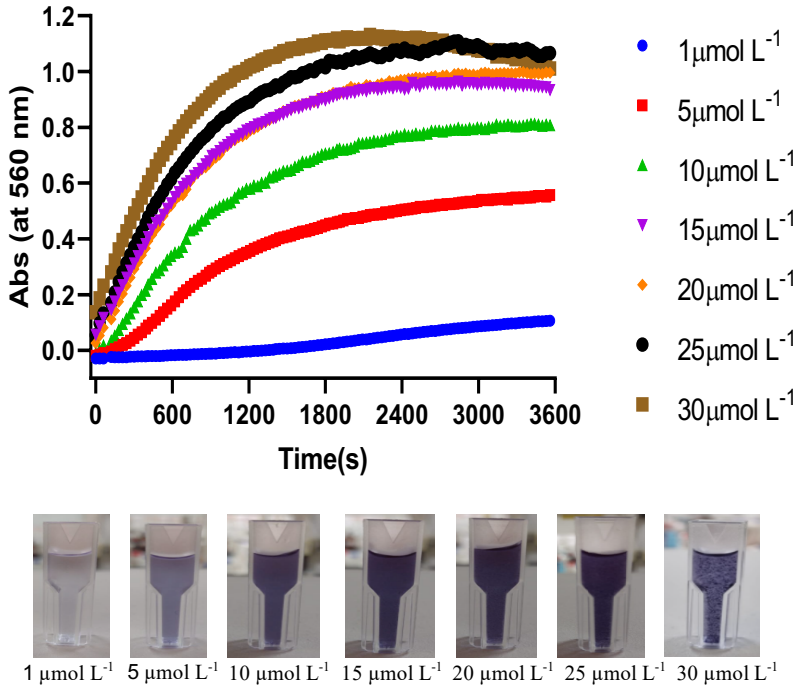

Figure S16. Kinetic curves corresponding to the spectral changes at 560 nm due to a reaction of **PR02** at 1 up to 30 µmol L^{-1} with 50 µmol L^{-1} NBT and 1.5 mmol L^{-1} glutathione (GSH), in 0.1 mol L^{-1} phosphate buffer at pH 7.4, spectrum obtained every 30 s for 3600s.

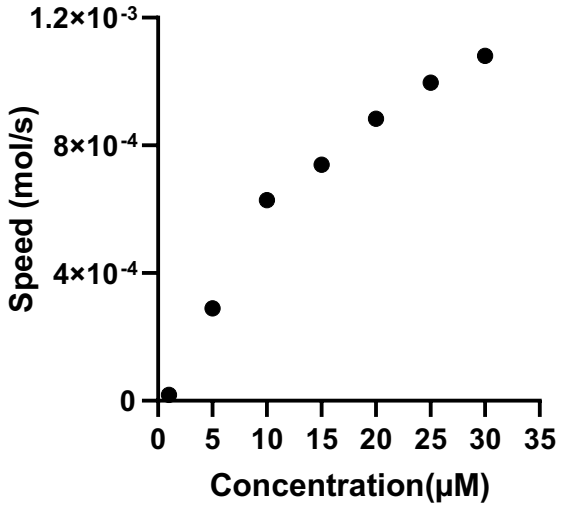

Figure S17. Superoxide generation in a dose dependent manner for **PR02** in reaction with 1.5 mmol L^{-1} of glutathione (GSH) monitored by 50 µmol L^{-1} of NBT as shown in Figure S16.

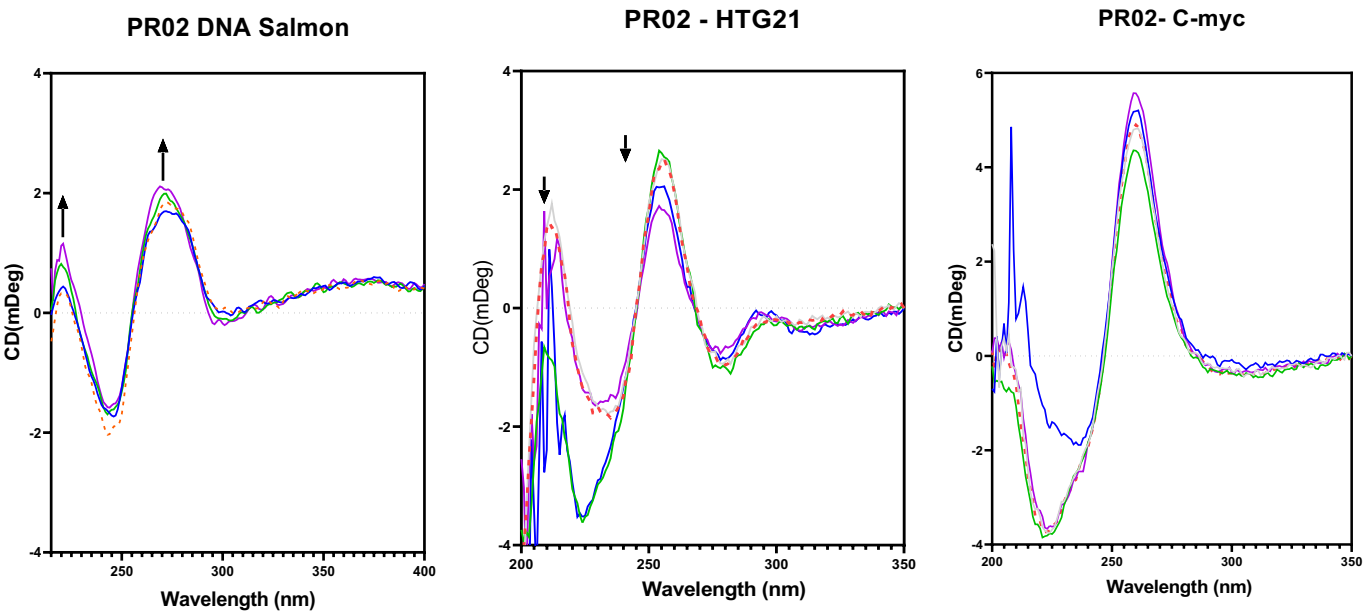

Figure S18. Circular dichroism of salmon DNA, G-quadruplexes DNAs 22AG and c-myc with **PR02** at concentrations from 6.25 µmol L^{-1} up to 50 µmol L^{-1}.

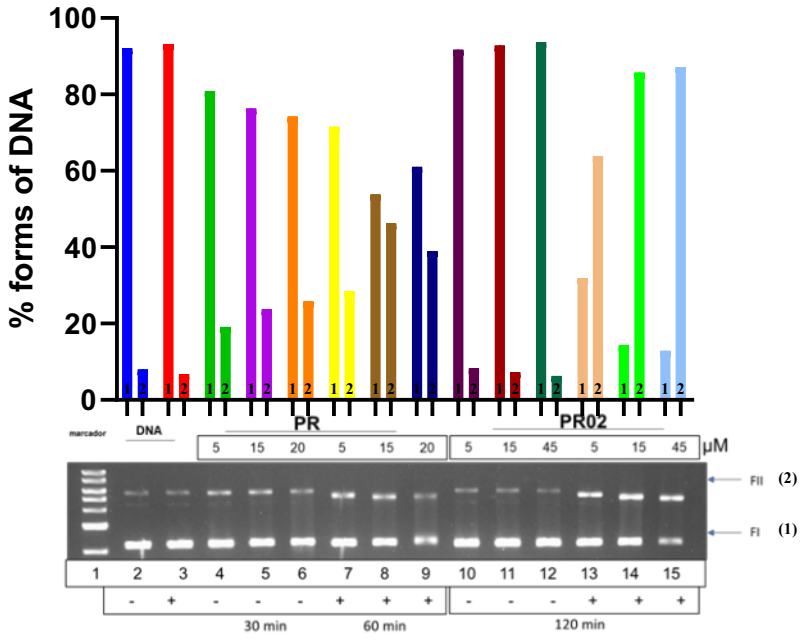

Figure S19. Photocleavage assay of pBR322 DNA (20 µM) in the presence of **PR** and **PR02** complexes at different concentrations in the dark and after irradiation with blue light (LED, λ_{max} = 460 nm). Lane 1: Linear DNA marker (ladder). Lane 2: pBR322 DNA only in the dark and Lane 3: pBR322 DNA only with light. Lanes 4 -15: metal complexes + pBR322 DNA at concentrations of 5, 15, 20 and 45 µmol L^{-1}. Lanes 7-9 and 13 to 15 were irradiated with blue LED, while others were kept in the dark.

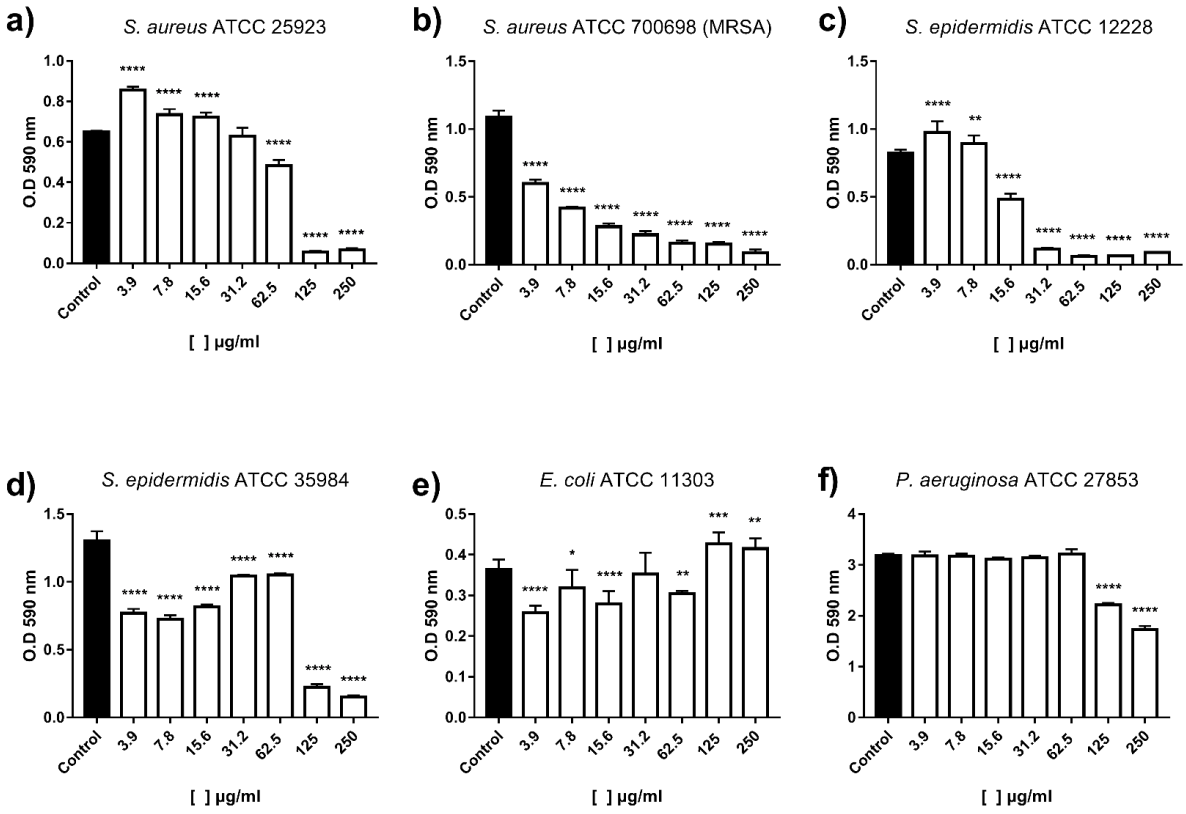

Figure S20. Effect of the **PR** complex on biofilm formation of *S. aureus*, *S. epidermidis*, *E. coli* and *P. aeruginosa*. Quantification of biomass of biofilms in formation (a to f). White bars represent bacteria treated with **PR**; black bars represent untreated bacteria. Error bars display SDs of the means. *$p < 0.05$, ** $p < 0.01$, *** $p < 0.001$ and **** $p < 0.0001$ compared to untreated controls. Samples light irradiated (λ_{max} = 463 nm) for 1 h, followed incubation.

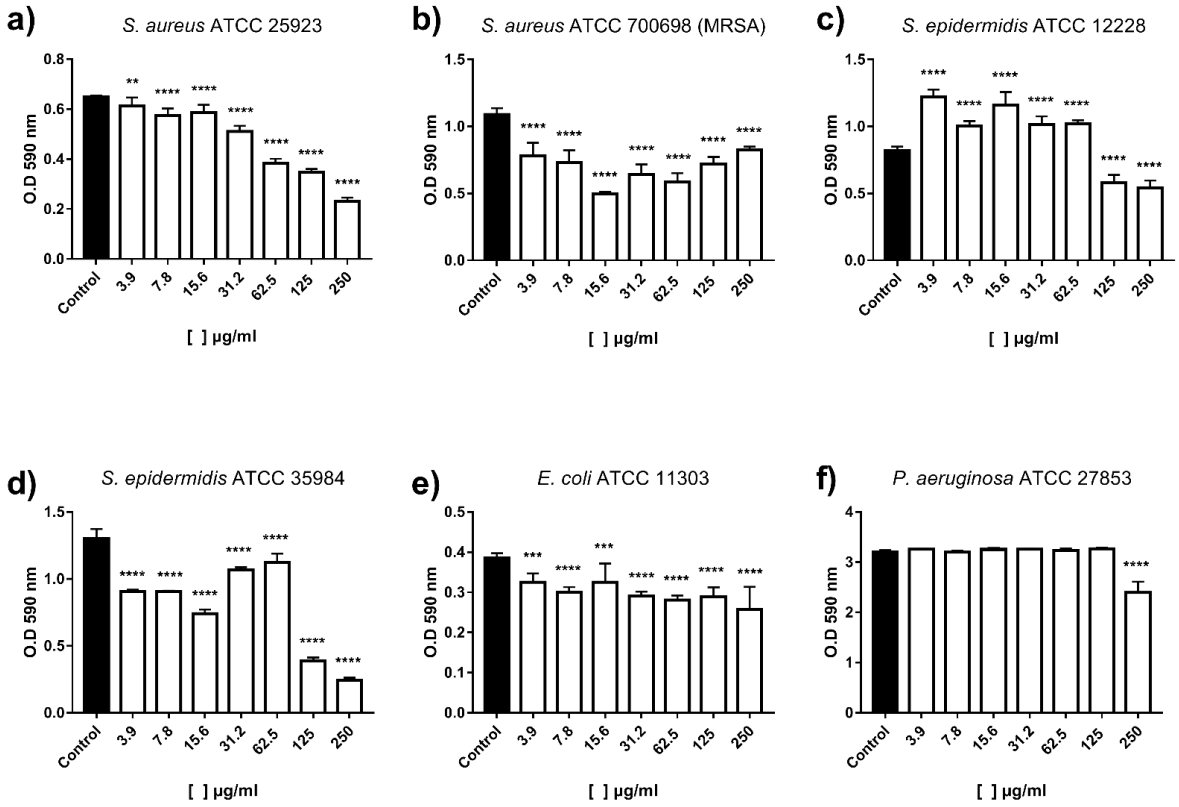

Figure S21. Effect of the **PR01** complex on the biofilm formation of *S. aureus*, *S. epidermidis*, *E. coli* and *P. aeruginosa*. Quantification of biomass of biofilms in formation (a to f). White bars represent bacteria treated with PR01; black bars represent untreated bacteria. Error bars display SDs of the means. *$p < 0.05$, ** $p < 0.01$, *** $p < 0.001$ and **** $p < 0.0001$ compared to untreated controls. Samples light irradiated (λ_{max} = 463 nm) for 1 h, followed incubation.

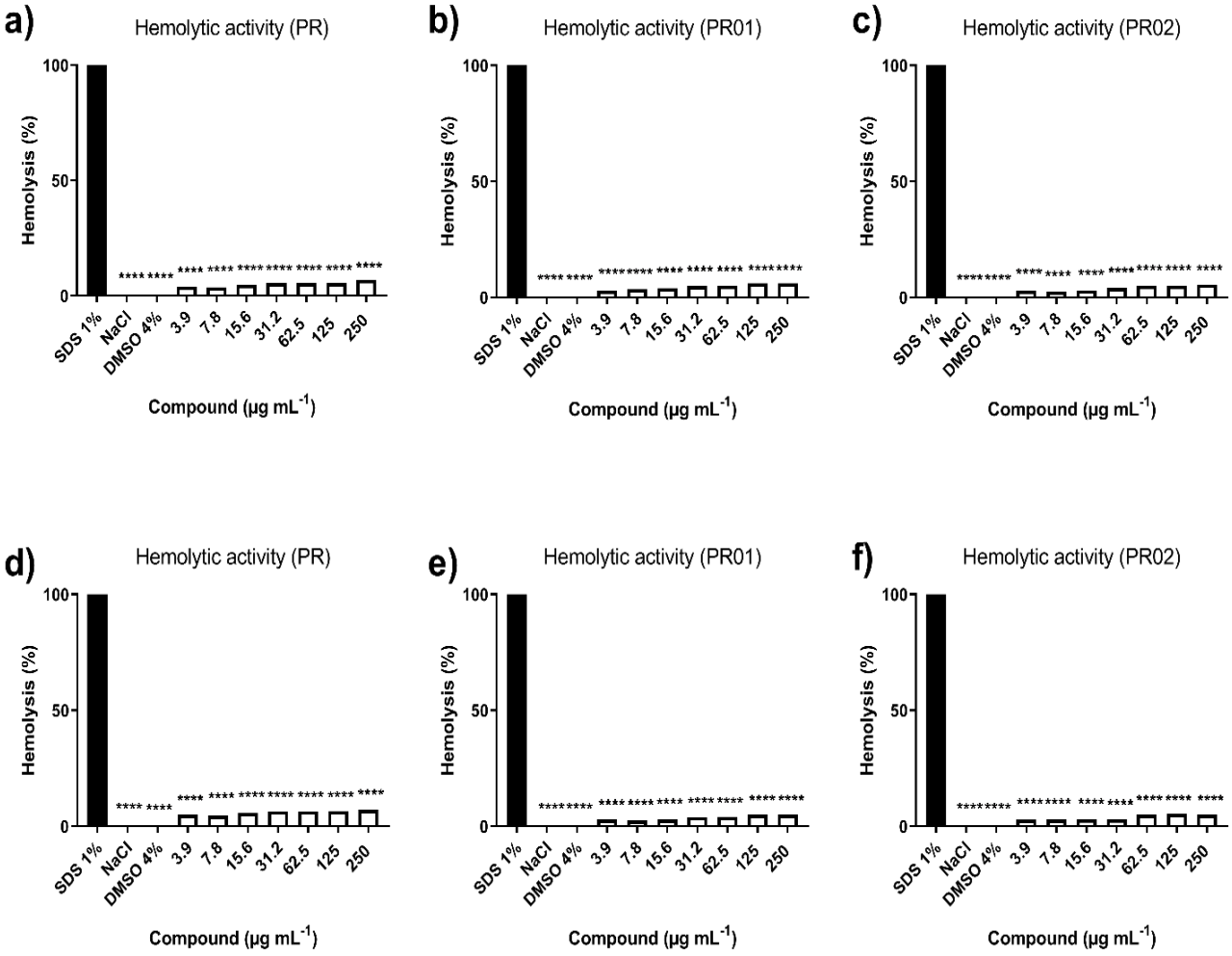

Figure S22. Hemolytic activity of **PR**, **PR01** and **PR02** ruthenium complexes without (a-c) and with light irradiation (d-e) (λ_{max} = 463 nm).

Table S1. Profile of Log P measurements

Ru complex		Log P	Reference
(PR)	$[Ru(bpy)(dppz)Cl_2]$	-0.26	This work
(PR01)	$Na[Ru(bpy)(dppz)SO_3NO_2]$	0.1	This work
(PR02)	$[Ru(bpy)(dppz)SO_3NO](PF_6)$	-0.17	This work
	$[Ru(bpy)_2(dppz)]Cl_2$	-2.5	[5]
	cis-$[Ru(bpy)_2(2\text{-MIM})(NO_2)]PF_6$	1.29	[6]

Table S2. Binding constant (K_b) for similar ruthenium complexes

Ru complex		K_b	Reference
(PR)	$[Ru(bpy)(dppz)Cl_2]$	6.90×10^4	This work
(PR01)	$Na[Ru(bpy)(dppz)SO_3NO_2]$	12.50×10^4	This work
(PR02)	$[Ru(bpy)(dppz)SO_3NO](PF_6)$	12.90×10^4	This work
	$[Ru(bpy)_2(dppz)]Cl_2$	320×10^4	[7]
	$[Ru(phen)_2(dppz)]Cl_2$	210×10^4	[8]
	$[Ru(bpy)_2(SO_3)NO](PF_6)$	0.79×10^4	[9]
	$[Ru(bpy)_2(SO_3)H_2O]$	10.41×10^4	[9]

1. Silva, F. O. N.; Araújo, S. X. B.; Holanda, A. K. M.; Meyer, E.; Sales, F. A. M.; Diógenes, I. C. N.; Carvalho, I. M. M.; Moreira, Í. S.; Lopes, L. G. F., Synthesis, Characterization, and NO Release Study of thecis- andtrans-[Ru(Bpy)2(SO3)(NO)]+ Complexes. *European Journal of Inorganic Chemistry* **2006,** *2006* (10), 2020-2026.
2. Silva, C. D. S.; Paz, I. A.; Abreu, F. D.; de Sousa, A. P.; Verissimo, C. P.; Nascimento, N. R. F.; Paulo, T. F.; Zampieri, D.; Eberlin, M. N.; Gondim, A. C. S.; Andrade, L. C.; Carvalho, I. M. M.; Sousa, E. H. S.; Lopes, L. G. F., Thiocarbonyl-bound metallonitrosyl complexes with visible-light induced DNA cleavage and promising vasodilation activity. *J Inorg Biochem* **2018,** *182*, 83-91.
3. da Silva, C. D. S. P., I. A.; Sousa, E. H. S.; Lopes, L. G. F.; , 2024.
4. Gouveia, F. S.; Silveira, J. A. D.; Holanda, T. M.; Marinho, A. D.; Ridnour, L. A.; Wink, D. A.; de Siqueira, R. J. B.; Monteiro, H. S. A.; de Sousa, E. H. S.; Lopes, L. G. D., New nitrosyl ruthenium complexes with combined activities for multiple cardiovascular disorders. *Dalton Transactions* **2023,** *52* (16), 5176-5191.
5. Puckett, C. A.; Barton, J. K., Methods to explore cellular uptake of ruthenium complexes. *Journal of the American Chemical Society* **2007,** *129* (1), 46-47.
6. de Oliveira Neto, J.; Marinho, M. M.; Silveira, J. A. M.; Rocha, D. G.; Lima, N. C. B.; Gouveia Junior, F. S.; Lopes, L. G. F.; de Sousa, E. H. S.; Martins, A. M. C.; Marinho, A. D.; Jorge, R. J. B.; Monteiro, H. S. A., Synthesis and potential vasorelaxant effect of a novel ruthenium-based nitro complex. *J Inorg Biochem* **2022,** *228*, 111666.
7. Burya, S. J.; Lutterman, D. A.; Turro, C., Absence of quenching by [Fe(CN)6]4- is not proof of DNA intercalation. *Chem Commun (Camb)* **2011,** *47* (6), 1848-50.
8. Ambroise, A.; Maiya, B. G., Ruthenium(II) complexes of 6,7-dicyanodipyridoquinoxaline: Synthesis, luminescence studies, and DNA interaction. *Inorganic Chemistry* **2000,** *39* (19), 4264-4272.
9. Martins, P. H. R.; Romo, A. I. B.; da Silva, F. O. N.; Nascimento, O. R.; Rodriguez-Lopez, J.; Diogenes, I. C. N.; Lopes, L. G. F.; Sousa, E. H. S., Reactivity of a nitrosyl ruthenium complex and its potential impact on the fate of DNA - An in vitro investigation. *J Inorg Biochem* **2023,** *238*, 112052.